Metallophysics and Advanced Technologies
Металофіз. новітні технол.
Metallofiz. Noveishie Tekhnol.
2022, vol. 44, No. 9, pp. 1077–1101
https://doi.org/10.15407/mfint.44.09.1077
Reprints available directly from the publisher

PACS numbers: 61.72.J-, 61.72.jj, 61.72.-y, 61.80.Jh, 61.82.Bg

A Study of Dislocation Loops Growth in Zr–Sn Alloys under Neutron Irradiation by Rate Theory Modelling

L. Wu, T. Xin, D. Kharchenko*, V. Kharchenko*, and O. Lysenko*

The First Institute, Nuclear Power Institute of China,
328, the 1st Section, Changshundadao Road,
Shuangliu, Chengdu, China
**Institute of Applied Physics, N.A.S. of Ukraine,*
58 Petropavlivska Str.,
40000 Sumy, Ukraine

We extend reaction rate theory to study dislocation loops growth and associated radiation growth in binary Zr–Sn alloys under neutron irradiation at reactor conditions. A model to describe experimental data for loops' number density is proposed. We discuss dose dependences of dislocation loop radii, their densities and growth strains and analyse an influence of irradiation temperature and sinks' strengths on statistical properties of loops. A competition between the interstitial and vacancy <*a*>-type loops is studied. Local loops distribution inside grains is analysed. Estimation of hardening of material is provided. Obtained results are compared with experimental observations.

Key words: zirconium alloys, defects, dislocation loops, growth strains, hardening.

Узагальнено теорію швидкости реакції для вивчення росту дислокаційних петель і пов'язаного з цим радіяційного розпухання в бінарних стопах Zr–Sn, опромінених нейтронами в реакторних умовах. Запропоновано модель для опису експериментальних даних стосовно густини дислокаційних петель. Обговорюються дозові залежності радіюсів дислокаційних петель, їхніх густин і ростових деформацій, а також аналізується вплив температури опромінення та потужностей стоків на статистичні

Corresponding author: Vasyl Kharchenko
E-mail: vasiliy@ipfcentr.sumy.ua

Citation: L. Wu, T. Xin, D. Kharchenko, V. Kharchenko, and O. Lysenko, A Study of Dislocation Loops Growth in Zr–Sn Alloys under Neutron Irradiation by Rate Theory Modelling, *Metallofiz. Noveishie Tekhnol.*, **44**, No. 9: 1077–1101 (2022). DOI: 10.15407/mfint.44.09.1077

властивості петель. Вивчається конкуренція між міжвузловими та вакансійними петлями <*a*>-типу. Проаналізовано розподіл локальних петель всередині зерен. Зроблено оцінку твердости матеріялу. Одержані результати порівняно з експериментальними даними.

Ключові слова: цирконійові стопи, дефекти, дислокаційні петлі, ростові деформації, зміцнення.

(Received July 22, 2022)

1. INTRODUCTION

As known, zirconium-based alloys used in modern reactors as cladding materials contain less than 2% of alloying elements such as tin, niobium, and others to improve mechanical properties and corrosion resistance of these materials [1, 2]. High-energy (> 1 MeV) neutron irradiation of these materials induces a development of dislocation structure resulting in a dimensional change of materials without applied stress known as radiation growth. This phenomenon is controlled by fluence, temperature, and material microstructure [3–7].

As usual, at neutron irradiation under reactor conditions (with temperature range (530–570) K and dose rate 10^{-7} dpa/s) the size of <*a*>-type loops (of interstitial and vacancy character with the Burgers vector $1/3 < 11\bar{2}0 >$) is around 10 nm. They emerge and grow from point defect clusters at extremely small doses ~ 10^{-3} dpa (displacements per atom). Loops of <*c*>-type lying in basal plane with Burgers vectors $1/2<0001>$ or $1/6 < 20\bar{2}3 >$ are of vacancy character. They emerge after critical dose of 3 dpa from two-dimensional vacancy platelets as loops precursors when their size overcomes a critical value [8]. These platelets have been observed in very particular conditions. It is possible that small impurity clusters are the form of basal platelets can act as nucleation sites for these loops [9, 10]. As was pointed out in [5] <*c*>-type loops appear as straight-line segments, they nucleate in collision cascades [11]. A size of these loops can exceed 200 nm. The number density of <*c*>-type loops is around 10^{15} cm^{-3} that is of one order less than one observes for <*a*>-type loops [3, 5].

From results of jointly conducted experimental and theoretic studies it was stated that radiation growth depends not only on irradiation conditions, but also on microstructure parameters: texture, grain size, point defect traps, defect mobility their diffusion anisotropy, and intra-granular effect (see review [7] and citations therein). A study of this phenomenon remains actual during several decades to predict a behaviour of cladding materials at different irradiation conditions.

As usual, in corresponding theoretical modelling one uses data obtained at different hierarchical levels allowing to capture main mechanisms, governing studied phenomenon and provide multi-scale or hy-

brid simulations including several methods operating on different levels of description. In order to get energetic parameters governing interaction of point defects and clusters with alloying elements and extended defects (dislocation lines, loops, grain boundaries) one usually exploits calculations from first principles [14–20]. Molecular dynamics and object kinetic Monte Carlo (OKMC) simulations (extending the time and length scale of molecular dynamics) give information about primary radiation damages and properties of defect clustering at elevated temperatures [21–26]. Cluster dynamics is used to receive data for cluster number density dynamics, mean cluster size and cluster growth speed at different irradiation regimes [27–29]. Phase field modelling allows one to describe defects rearrangement and phase stability based on thermodynamic approaches and reaction rate theory [6, 25, 30–38].

However, despite a progress in studying radiation growth, there are some discrepancies between experimental data and results coming from growth prediction models [7]. Mostly it is related to mean field approximation by neglecting some microstructural properties and statistical correlations between micro- and macrostructures. Moreover, most of the results were obtained for single crystals, whilst real materials are poly-crystalline and loops can be locally arranged inside grains due to grain boundary effect on migrating defects. Additionally, it was shown recently that both kinds of point defects in zirconium-based alloys manifest diffusion anisotropy that results in continuous development of this approach to get more accurate results predicting materials behaviour [36, 37, 39].

In this paper, we focus our attention on a further development of the rate theory by studying dynamics of dislocation loop and radiation growth in Zr–Sn systems under neutron irradiation at reactor conditions. We generalize the rate theory for radiation damages in Zr–Sn alloys based on previously derived models [6, 35–37, 40, 41]. The novelty of the model is in the using a continuous dynamic of both $<a>$- and $<c>$-type loop number densities by exploiting main mechanisms of cluster dynamics [27–29] with verification of obtained results. Comparing to previously used approach [35, 36] the proposed model admits a continuous change of growth rates of loop number densities by including physically based mechanisms and experimental data. Moreover, a small set of fitting parameters can be used to relate experimentally observed data with results of modelling at different irradiation conditions. Here we take into account production biased model and effect of domains inside grains resulting in loops growth rate change together with local description of loop increase inside grains. The proposed model allows one to describe local distribution of growth strains inside grains at different irradiation conditions and sink strengths. It will be shown that both interstitial and vacancy $<a>$-type loops com-

pete with each other and govern growth strains dynamics. By using obtained data, we study dose and parametric dependences of the radiation-induced hardening.

The paper is organized in the following manner. In Section 2, we describe generalized mathematical model for loop radii and growth strains dynamics. In Section 3, we discuss dose dependences of main studied quantities and provide comparison with experimental data. We conclude in Section 4.

2. MODEL

2.1. Rate Equations

We start from the standard model describing point defects dynamics discussed in [40], where for time-dependent point defect concentrations we use a notation $c_{\mathrm{i,v}}$, where subscripts i and v relate to interstitials and vacancies, respectively. As far as tin atoms serve as traps for vacancies, next we introduce c_{vT} as a concentration of trapped vacancies. In our study, we take into account that defect clusters can emerge simultaneously together with Frenkel pairs. Concentration interstitial and vacancy clusters we denote by $c^{j}_{\mathrm{q\ cl}}$, where q = {i, v}, j is the crystallographic direction ($j = \{m, c\}$, $m = \{a1, a2, a3\}$). Generally, these clusters can be sessile and glissile and are able to emit point defects. Such clusters are embryos of loops and can govern dynamics of their growth. We admit that an efficiency of absorbing clusters by grain boundaries depends on a distance between clusters and grain boundaries. Rate theory equations for point defect concentrations should be accompanied by equations describing dynamics of glissile cluster concentration as follows [6, 40]:

$$
\begin{aligned}
&\partial_t c_{\mathrm{i}} = K_{\mathrm{i}} - D_{\mathrm{i}} k_{\mathrm{i}}^2 (c_{\mathrm{i}} - c_{\mathrm{i0}}) - \alpha_{\mathrm{r}} c_{\mathrm{v}} c_{\mathrm{i}} + K_{\mathrm{e(i)\ cl}},\\
&\partial_t c_{\mathrm{v}} = K_{\mathrm{v}} - D_{\mathrm{v}} k_{\mathrm{v}}^2 (c_{\mathrm{v}} - c_{\mathrm{v0}}) - \alpha_{\mathrm{r}} c_{\mathrm{v}} c_{\mathrm{i}} + K_{\mathrm{e}}^{\mathrm{T}} + K_{\mathrm{e(v)\ cl}},\\
&\partial_t c_{\mathrm{vT}} = D_{\mathrm{v}} k_{\mathrm{vT}}^2 c_{\mathrm{v}} - D_{\mathrm{i}} k_{\mathrm{iT}}^2 c_{\mathrm{i}} c_{\mathrm{vT}} - K_{\mathrm{e}}^{\mathrm{T}},\\
&\partial_t c^{j}_{\mathrm{q\ cl}} = \frac{K \varepsilon_{\mathrm{q}}^{g}}{d_{\mathrm{q}} n_{\mathrm{q}}} - D^{j}_{\mathrm{q\ cl}} S^{j}_{\mathrm{q\ cl}}(l) c^{j}_{\mathrm{q\ cl}} - K_{\mathrm{eq\ cl}}.
\end{aligned}
\tag{1}
$$

Here, $K_{\mathrm{q}} = K(1 - \varepsilon_{\mathrm{q}})$ relates to production rate of the corresponding point defects due to irradiation, where $K \equiv K_{\mathrm{NRT}}(1 - \varepsilon_{\mathrm{r}})$, K_{NRT} is the dose rate defined according to the NRT standard [42], ε_{r} relates to cascade recombination efficiency, $(1 - \varepsilon_{\mathrm{q}})$ denotes the fraction of free (unclustered) point defects, $\varepsilon_{\mathrm{q}} = \varepsilon_{\mathrm{q}}^{g} + \varepsilon_{\mathrm{q}}^{s}$, $\varepsilon_{\mathrm{q}}^{g}$ and $\varepsilon_{\mathrm{q}}^{s}$ are efficiencies of generation of glissile and sessile clusters, respectively. The second terms in first two equations are responsible for point defects annihilation at

sinks of strength k_q^2, D_q corresponds to defect diffusivity, c_{q0} denotes the equilibrium defect concentration, as usual. Processes of defects recombination are governed by the rate constant $\alpha_r = 4\pi r_0(D_i + D_v)/\Omega$, where r_0 and Ω are recombination radius of point defects and atomic volume, respectively. In the equation for trapped vacancies, one considers their production when vacancies find traps (the first term), recombination with free interstitials (second term) and emission of free vacancies from traps with the rate K_e^T (the last term). Such emission increases a number of free vacancies (see the fourth term in equation for c_v). Quantities k_{vT}^2 and k_{iT}^2 describe the corresponding trap sink strengths. In the equation for clusters d_q is the number of directions along which i/v-clusters can be formed; n_q is the number of defects in the corresponding cascade-produced mobile cluster; $D_{q\,cl}^j$ relates to diffusivity of clusters; $S_{q\,cl}^j(l)$ is the corresponding sink strength depending on a distance from the grain boundary, l. Terms $K_{eq\,cl} = \sum_j K_{eq\,cl}^j$ describe contribution from defects due to their emission from clusters.

We assume that all sinks are smeared over the whole system, not localized. For sink strengths one can write: $k_q^2 = k_{qN}^2 + k_{GB}^2 + k_{q\,T}^2 + k_{qL}^2$. The quantity $k_{qN}^2 = \sum_j Z_{qN}^j \rho_N^j$ is related to network line dislocations with the density ρ_N^j in each crystallographic direction j and efficiency $Z_{qN}^j = Z_{qN}$ of dislocations to absorb defects of each sort. The sink strength $k_{GB}^2 = \sum_{jn} Z_{n\,GB} / \lambda_{n\,GB}^2$ describes an effect of grain boundaries, where $\lambda_{n\,GB}$ is the grain size in one of three Cartesian directions $n = (x, y, z)$. Bias coefficient Z_{GB}^n is taken according to the definition noted in Refs. [6, 36, 43]. Next, for simplicity, we assume $\lambda_{n\,GB} = \lambda_{GB}$ resulting to $Z_{n\,GB}^j = Z_{n\,GB}$. Sinks strengths k_{iT}^2 and k_{vT}^2 are taken from [44]: $k_{qT}^2 = Z_{qT} 4\pi r_T N_{Zr}$; the corresponding bias coefficients take the form: $Z_{iT} = c_T f / [(r_T / b)^3 + f]$, $Z_{vT} = c_T(1 - f) / [1 + (r_T / b)^3 - f]$, where traps are assumed as spherical substances with mean capture radius r_T comparable with the Burgers vector value b, N_{Zr} is the atomic number density of zirconium (as matrix element), $f = c_{vT}/c_T$ is the trap occupation probability. As assumed, vacancy relax the accumulated energy at the trap and hence, they are captured with a binding energy E_T^B. Thermal emission of vacancies is defined through the rate: $K_e^T = D_v k_{vT}^2 \beta_v [f / (1 - f)] \exp(-E_T^B / T)$, $\beta_v = 7.0$ is the geometric factor [40, 44]. As shown, the upper limit for the trap occupation probability for Zr–1.5% Sn can be obtained if at least ~ 6% of traps are occupied with concentration of solute-trap complexes ~ 0.1% [40]. As far as Sn atoms serve as traps it means that one relates concentration of Tin, c_{Sn} to the concentration of traps c_T as $c_T = 0.06 c_{Sn}$. Sinks strengths k_{iL}^2 and k_{vL}^2 are related to dislocation loops of different type. We take into account that interstitial loops are possible only in $m = \{a1, a2, a3\}$ directions, whereas vacancy loops can be observed in all $j = 4$ crystallographic directions. Moreover, <c>-type vacancy loops are possible only at doses exceeding 3 dpa. For these sink strengths one can write

$k^2_{\mathrm{qL}} = \sum_m (Z^{\mathrm{m}}_{\mathrm{qI}}\rho^{\mathrm{m}}_{\mathrm{I}} + Z^{\mathrm{m}}_{\mathrm{qV}}\rho^{\mathrm{m}}_{\mathrm{V}}) + Z^{\mathrm{c}}_{\mathrm{qV}}\rho^{\mathrm{c}}_{\mathrm{V}}$. For loop densities one has the standard definition $\rho^j_{\mathrm{I,V}} = 2\pi R^j_{\mathrm{I,V}} N^j_{\mathrm{V}}$, , where $R^j_{\mathrm{I,V}}$ and $N^j_{\mathrm{I,V}}$ denote the corresponding loop radius and loop number density, respectively. In the considered model we use functional dependences of bias factors $Z^m_{\mathrm{q},\Upsilon} = Z^m_{\mathrm{q},\Upsilon}(R^m_\Upsilon)$ according to [6, 45, 46], where $\Upsilon = \{\mathrm{I}, \mathrm{V}\}$, $Z_{n\,\mathrm{GB}} >> Z^m_{\mathrm{iI}} \geq Z^j_{\mathrm{iV}} > Z^m_{\mathrm{vI}} \geq Z^j_{\mathrm{vV}} > Z^j_{\mathrm{iN}} \geq Z^j_{\mathrm{vN}}$, $Z^j_{\mathrm{iN}} = 1.1$, $Z^j_{\mathrm{vN}} = 1.0$.

We take into account that the sink strength of defect clusters $Z^j_{\mathrm{q\,cl}}$ depends on the distance l from the grain boundary as follows [6, 41]:

$$Z^j_{\mathrm{q\,cl}}(l) = 2(\pi r_{\mathrm{q\,cl}}\tilde{\rho}^j_{\mathrm{q}} / 2)^2,\ \tilde{\rho}^j_{\mathrm{q}} = \rho^j + 2(\pi r_{\mathrm{q\,cl}}\sqrt{l(2\lambda_{\mathrm{GB}} - l)})^{-1},$$

where $r_{\mathrm{q\,cl}}$ is the capture radius of loops for mobile clusters, $\rho^j = \rho^j_{\mathrm{N}} + \rho^j_{\mathrm{V}} + \rho^j_{\mathrm{I}}$, with $\rho^{\mathrm{c}}_{\mathrm{I}} = 0$ (no interstitial loops are possible in basal plane).

To obtain dynamical equations for interstitial/vacancy (I/V)-loop size $R^j_{\mathrm{I,V}}$ one uses the standard technique [6] and gets

$$\begin{aligned}
b^m\partial_t R^m_{\mathrm{I}} &= g^m_{\mathrm{I}}[Z^m_{\mathrm{iI}}D_{\mathrm{i}}c_{\mathrm{i}} - Z^m_{\mathrm{vI}}D_{\mathrm{v}}(c_{\mathrm{v}} - c^m_{\mathrm{iL}}) + \\
&+ \frac{K(\pi r_{\mathrm{i\,cl}})^2\tilde{\rho}^m}{2}\left(\frac{\varepsilon_{\mathrm{ig}}}{d_{\mathrm{i}}S^m_{\mathrm{i\,cl}}(l)} - \frac{\varepsilon_{\mathrm{vg}}}{d_{\mathrm{v}}S^m_{\mathrm{v\,cl}}(l)}\right) - \frac{b^m R^m_{\mathrm{I}}}{2N^m_{\mathrm{I}}}\partial_t N^m_{\mathrm{I}}], \\
b^m\partial_t R^m_{\mathrm{V}} &= g^m_{\mathrm{V}}[Z^m_{\mathrm{vV}}D_{\mathrm{v}}(c_{\mathrm{v}} - c^m_{\mathrm{vL}}) - Z^m_{\mathrm{iV}}D_{\mathrm{i}}c_{\mathrm{i}} + \\
&+ \frac{K(\pi r_{\mathrm{v\,cl}})^2\tilde{\rho}^m}{2}\left(\frac{\varepsilon_{\mathrm{vg}}}{d_{\mathrm{v}}S^m_{\mathrm{v\,cl}}(l)} - \frac{\varepsilon_{\mathrm{ig}}}{d_{\mathrm{i}}S^m_{\mathrm{i\,cl}}(l)}\right) - \frac{b^m R^m_{\mathrm{V}}}{2N^m_{\mathrm{V}}}\partial_t N^m_{\mathrm{V}}], \qquad (2) \\
b^{\mathrm{c}}\partial_t R^{\mathrm{c}}_{\mathrm{V}} &= g^{\mathrm{c}}_{\mathrm{V}}[Z^{\mathrm{c}}_{\mathrm{vV}}D_{\mathrm{v}}(c_{\mathrm{v}} - c^{\mathrm{c}}_{\mathrm{vL}}) - Z^{\mathrm{c}}_{\mathrm{iV}}D_{\mathrm{i}}c_{\mathrm{i}} + \frac{K(\pi r_{\mathrm{v\,cl}})^2\tilde{\rho}^{\mathrm{c}}\varepsilon_{\mathrm{vg}}}{2d_{\mathrm{v}}S^{\mathrm{c}}_{\mathrm{v\,cl}}(l)} - \frac{b^{\mathrm{c}}R^{\mathrm{c}}_{\mathrm{V}}}{2N^c_{\mathrm{V}}}\partial_t N^{\mathrm{c}}_{\mathrm{V}}].
\end{aligned}$$

For concentration of vacancies, which are in equilibrium with vacancy- and interstitial-type loops, one exploits the standard definition [6].

In equations for loop radii, we introduce growth scaling functions $g_{\mathrm{I,V}}(t)$ to take into account a transformation of evolving dislocation loops into a low-energy cellular dislocation structure according to discussions given in [47]. As known, this structure forms domains of the size $L^j_{\mathrm{d}} = L^0_{\mathrm{d}}(\rho^j_{\mathrm{N}})^{-1/2}$, where $L^0_{\mathrm{d}} = C_A C_\rho(\pi / f(\upsilon))^{1/2}$, $C_A = 3$, $C_\rho \approx 1$, $f(\upsilon) = (1 - \upsilon / 2) / (1 - \upsilon)$ [48]. For growth scaling functions one admits $g^j_{\mathrm{I,V}} = 1 - 2R^j_{\mathrm{I,V}}(\rho^j_{\mathrm{I,V}})^{1/2} / L^0_{\mathrm{d}}$. It is able to prevent loop size growth up to sizes exceeding domain size. It allows one to describe processes of loops annihilation with dislocation network of cellular structure by delaying corresponding dynamics.

To get a close loop system one needs to know an equation for the loop number density $N_{\mathrm{I,\,V}}$ modelling loop nucleation processes. To this end, one can use the experimental observation for nucleation of loops. As

known, <*a*>-loops nucleate from beginning of irradiation and reach typical values ~ 10^{16} cm^{-3} after several dpa, whereas vacancy <*c*>-loops nucleate above a critical dose ≈ 3 dpa and attain density ~ 10^{15} cm^{-3} [49, 50–52]. A simplest model for evolution of the loop number density was proposed in [35]. Its modification by fitting experimental data from OSIRIS reactor was done in [36]. The simplest model can adequately explain experimental data for loops nucleation but cannot describe temperature dependences of measured quantities.

In our approach, we use a dynamical model based on propositions discussed in [47]. To describe the loop number densities in <*a*>-directions one can use an equation of the form:

$$\partial_t N_{\mathrm{I}}^m = \frac{K_{\mathrm{i}}\Phi(T,K)}{\pi b^m (R_{\mathrm{I}}^m(0))^2} - \frac{N_{\mathrm{I}}^m}{\tau_{\mathrm{I}}^m} + \frac{\sqrt{2}D_{\mathrm{i}}c_{\mathrm{i}}^2}{2\Omega^{5/3}} - \frac{b^m D_{\mathrm{v}} c_{\mathrm{v}} N_{\mathrm{I}}^m}{< R_{\mathrm{I}} > \Omega^{2/3}}. \qquad (3)$$

Here, first two terms are responsible for short time dynamics. The first one is related to cluster production in cascades with initial cluster size $R_{\mathrm{I}}^m(0) = (n_{\mathrm{i}0}\Omega / \pi b_m)^{1/2}$, where $n_{\mathrm{i}0}$ is the number of defects in the cluster at loop creation. The function $\Phi(T, K)$ gives temperature and dose rate fit of experimental data and is responsible for maximal values of N_{I}^m. As was shown in [53] the temperature dependence of loop number density for zirconium alloys can be described as $\Phi(T, K) = N_0(K)/(1 + 7.2\cdot 10^{18}\exp(-Q_{\mathrm{a}}/RT))$, where $Q_{\mathrm{a}} = 55320$ cal/mol is the activation energy for self-diffusion, $N_0(K)$ is the fitting parameter depending on the dose rate. The second term corresponds to the cluster life-time $\tau_{\mathrm{I}}^m = L_{\mathrm{d}}^m / 2v_{\mathrm{I}}^m$, where the cluster growth speed is defined in the standard way as $v_{\mathrm{I}}^m = (Z_{\mathrm{iI}}D_{\mathrm{i}}c_{\mathrm{i}} - Z_{\mathrm{vI}}D_{\mathrm{v}}c_{\mathrm{v}}) / b^m$. By considering so-called relaxation regime one gets $D_{\mathrm{q}}c_{\mathrm{q}} \approx K_{\mathrm{q}} / k_{\mathrm{q}}^2$ that leads to approximation:

$$v_{\mathrm{I}}^m = \frac{K_{\mathrm{i}} Z_{\mathrm{iI}}^0}{b^m k_{\mathrm{i}}^2 Z_{\mathrm{iN}}}\left[1 - \frac{K_{\mathrm{v}}}{K_{\mathrm{i}}}\frac{Z_{\mathrm{vI}}^0}{Z_{\mathrm{iI}}^0}\frac{Z_{\mathrm{iN}}}{Z_{\mathrm{vN}}}\frac{k_{\mathrm{i}}^2}{k_{\mathrm{v}}^2}\right],$$

where Z_{qI}^0 is calculated for the clusters of the size $R_{\mathrm{I}}^m(0)$. In this regime one can consider dislocations as main sinks of point defects, *i.e.*, one can put $\rho_{\mathrm{N}}^m >> \rho_{\mathrm{I}}^m$. Last two terms in Eq. (3) are responsible for long time dynamics: creation of clusters by interaction of interstitials and loss of loops due to absorption of vacancies, where the mean loop radius is $3 < R_{\mathrm{I}} >= \sum_m R_{\mathrm{I}}^m$. This formalism can be used to describe vacancy cluster formation in *m* direction. Next, we put $N_{\mathrm{I}}^m = N_{\mathrm{V}}^m$ for simplicity.

For the number of vacancy loops in <*c*>-direction one can use a model described in [35]. Generally, the model for <*c*>-type loop number density is quite complicated, here one can issue several stages in its dynamics: incubation stage at doses up to 3 dpa, growth stage and qua-

si-stationary stage. From the other hand, one can use experimental data to get a dose-fitting curve. Some simplification of that model can be done by using so-called dose-response (DoseResp) curve with variable hill-slope (belonging to a set of logistic type functions) allowing to fit experimental data for <*c*>-type loops number density at different doses and irradiation conditions. By using standard definition of this function, one can get dynamical equation of the form

$$\partial_t N_{\mathrm{I}}^{\mathrm{c}} = \frac{N_{\mathrm{V}}^{\mathrm{c,\,max}}(T)K}{\phi^*} \frac{\exp[(\phi_m - \phi)/\phi^*]}{(1+\exp[(\phi_m - \phi)/\phi^*])^2}, \tag{4}$$

where $\phi = Kt/(1-\varepsilon_{\mathrm{r}})$ is the accumulated dose, ϕ_m is the dose related to the centre of the slope, ϕ^* defines the hill slope, $N_{\mathrm{V}}^{\mathrm{c,\,max}}(T)$ controls the maximal value of the loop number density. This model gives good approximation for experimental data [54].

To compute strains associated with loop growth in all directions we calculate the climb velocity as a function of the net flux of defects arriving at dislocations [35, 36] and use the Orowan relation to get equations for strain rates in each crystallographic directions in the form:

$$\begin{aligned}
\partial_t e^m &= K\left(\frac{\varepsilon_{\mathrm{i}}}{3} - \frac{\varepsilon_{\mathrm{v}}}{4}\right) - \sum_n Z_{n\,\mathrm{GB}}^m \lambda_{\mathrm{GB}}^{-2}[D_{\mathrm{v}}(c_{\mathrm{v}} - c_{0\mathrm{v}}) - D_{\mathrm{i}}c_{\mathrm{i}}] - \rho_{\mathrm{N}}^m[Z_{\mathrm{vN}}^m D_{\mathrm{v}}(c_{\mathrm{v}} - c_{0\mathrm{v}}) - \\
&- Z_{\mathrm{iN}}^m D_{\mathrm{i}}c_{\mathrm{i}}] - \rho_{\mathrm{I}}^m[Z_{\mathrm{vI}}^m D_{\mathrm{v}}(c_{\mathrm{v}} - c_{\mathrm{iL}}) - Z_{\mathrm{iI}}^m D_{\mathrm{i}}c_{\mathrm{i}}] - \rho_{\mathrm{V}}^m[Z_{\mathrm{vV}}^m D_{\mathrm{v}}(c_{\mathrm{v}} - c_{\mathrm{vL}}) - Z_{\mathrm{iV}}^m D_{\mathrm{i}}c_{\mathrm{i}}], \\
\partial_t e^{\mathrm{c}} &= -\frac{K\varepsilon_{\mathrm{v}}}{4} - \sum_n Z_{n\,\mathrm{GB}}^{\mathrm{c}} \lambda_{\mathrm{GB}}^{-2}[D_{\mathrm{v}}(c_{\mathrm{v}} - c_{0\mathrm{v}}) - D_{\mathrm{i}}c_{\mathrm{i}}] - \rho_{\mathrm{N}}^{\mathrm{c}}[Z_{\mathrm{vN}}^{\mathrm{c}} D_{\mathrm{v}}(c_{\mathrm{v}} - c_{0\mathrm{v}}) - \\
&- Z_{\mathrm{iN}}^{\mathrm{c}} D_{\mathrm{i}}c_{\mathrm{i}}] - \rho_{\mathrm{V}}^{\mathrm{c}}[Z_{\mathrm{vV}}^{\mathrm{c}} D_{\mathrm{v}}(c_{\mathrm{v}} - c_{\mathrm{vL}}) - Z_{\mathrm{iV}}^{\mathrm{c}} D_{\mathrm{i}}c_{\mathrm{i}}].
\end{aligned} \tag{5}$$

The derived formalism for loop radii dynamics and growth strains calculations generalizes approaches discussed in works [35, 36, 55] for calculation radiation growth in zirconium based alloys by taking into account bias coefficients for each kind of loops, grain boundaries and distance from the grain boundaries. By using formalism described in [35, 36] one gets strains and dislocation densities in Cartesian axes.

Dislocations, dislocation loops, grain boundaries act as obstacles to dislocation motion resulting in dispersed-barrier hardening of irradiated materials. The change in shear stress $\Delta\tau_{\mathrm{tot}}$ required to unpin dislocations from obstacles defines the yield strength $\Delta\sigma_Y = M_{\mathrm{Zr}}\Delta\tau_{\mathrm{tot}}$, where $M_{\mathrm{Zr}} = 3.5$ is the Taylor factor [56]. The total hardening from all obstacles is described by the change in the shear stress [57]: $\Delta\tau_{\mathrm{tot}} = (\sum_\sigma \Delta\tau_\sigma^2)^{1/2}$, where the sum is taken over all obstacles: network of dislocations ($\sigma = \mathrm{N}$), grain boundaries ($\sigma = \mathrm{GB}$), dislocation loops of both <*a*>- and <*c*>-types ($\sigma = L_{\mathrm{I}}^{\alpha}, \sigma = L_{\mathrm{V}}^{\alpha}, \sigma = L_{\mathrm{I}}^{\mathrm{c}}$).

A contribution from network of dislocation is [57] $\Delta\tau_{\mathrm{N}} = \alpha_{\mathrm{d}}\mu b^{\mathrm{a}}(\tilde{\rho}_{\mathrm{N}})^{1/2}$, where $\tilde{\rho}_{\mathrm{N}} = \sum_j (b^j / b^{\mathrm{a}})^2 \rho_{\mathrm{N}}^j$ is the total dislocation density, μ is the shear modulus, and $\alpha_{\mathrm{d}} = 0.2$ is the dislocation-

dislocation interaction parameter that determines the strength of the barrier to dislocation motion. Grain boundaries effect is expressed as follows [56]: $\Delta\tau_{GB} = (C_{Zr} / M_{Zr})\lambda_{GB}^{-1/2}$, where $C_{Zr} = 200$ MPa·μm$^{1/2}$ is taken for pure zirconium [58]. Dislocation loops hardening is described by the dispersed-barrier hardening model [59]: $\Delta\tau_{L_\Upsilon^m} = \alpha_{L^m}\mu b^m(2 < R_\Upsilon^m > N^a)^{1/2}$, $\Delta\tau_{L_V^c} = \alpha_L^c\mu b^c(2 < R_V^c > N^c)^{1/2}$, where computations are provided by considering mean dislocation radius $< R_{\{\}}^j >$. The corresponding barrier strengths $\alpha_{L_\Upsilon^m}$ and α_L^c are loop size dependent functions as was discussed in [59]. Here we consider a mixed case of screw and edge dislocations.

2.2. Assumptions Used at Modelling

In this study we assume that traps are immobile (Sn atom is oversized comparing to atom of matrix) and diffusion of point defect is described mostly by diffusivities of point defects in pure Zr with corrections caused by traps presence. Therefore, further, without loss of generality, one can assume $D_i \approx D_i^{Zr}$, and for the vacancy diffusivity, we use formula obtained in [63]:

$$D_v = D_i^{Zr}\left[1 - \frac{c_{Sn}}{c_{Sn} - c_{v0} + \exp(-E_d / T)}\right],$$

where for vacancy-solute complex dissociation energy we put $E_d \approx E_T^B$.

As known, the point defects diffuse anisotropically in pure Zr and in Zr-based alloys [15, 39, 60, 61, 63, 64]. The significance of the diffusion anisotropy was confirmed by OKMC simulations [39] to describe radiation growth. At the same time, a question about anisotropic diffusion of point defects remains debatable in literature and the most of theoretic reaction rate models incorporates assumptions of isotropic vacancy diffusion and anisotropic interstitials diffusion.

In our approach, we use so-called Diffusional Anisotropy Difference (DAD) model [60], which is still popular within the scientific community probably because of its simplicity and its explanatory capacity. It allows us to relate our results to previously published [35, 36]. Their accuracy depends of course on a set of other microscopic parameters (defect clustering efficiencies), fitting parameters and limitation of model when one considers defect cluster concentration instead of introducing dynamics of di-, tri-, tetra-, and, at least, penta-defect clusters. The main idea here is to capture main results able to describe locality of loops distribution inside grains by using data for loop number densities from experiments.

Generally, one can consider the mean diffusion coefficient for point defects as $D_q^{Zr} = ([D_{qa}^{Zr}]^2 D_{qc}^{Zr})^{1/3}$, where D_{qa}^{Zr} and D_{qc}^{Zr} are diffusion coefficients along *a* and *c* axis [65, 21, 22]. Following DAD model [28, 60]

TABLE 1. Material parameters used in simulation.

Parameter	Value	Dimension	Ref.
Lattice parameters for Zr (a, c)	$(3.2, 5.13)\cdot 10^{-8}$	cm	
Atomic volume (Ω)	$3.32\cdot 10^{-23}$	cm^3	
Equilibrium vacancy concentration (c_{v0})	$0.54e^{-1.8\mathrm{eV}/k_BT}$	at. fract.	[66]
Equilibrium interstitial concentration (c_{i0})	$e^{-4.0\mathrm{eV}/k_BT}$	at. fract.	[40]
Thermal diffusivity of vacancies (D_v^{Zr})	$2.2\cdot 10^{-2}e^{-0.93\mathrm{eV}/k_BT}$	cm^2/s	[28]
Diffusivity of interstitials in c-direction (D_{ic}^{Zr})	$4.7\cdot 10^{-4}e^{-0.15\mathrm{eV}/k_BT}$	cm^2/s	[28]
Diffusivity of interstitials in a-direction (D_{ia}^{Zr})	$3.5\cdot 10^{-4}e^{-0.06\mathrm{eV}/k_BT}$	cm^2/s	[28]
Trap-vacancy binding energy (E_T^B)	0.3	eV	[40]
Stacking fault energy ($\gamma_{SF}^a, \gamma_{SF}^c$)	$9.05\cdot 10^{13}$, $1.242\cdot 10^{14}$	eV/cm^2	[67]
Maximal number density ($N_V^{c,max}$)	$8\cdot 10^{15}$	cm^{-3}	
Fitting parameter N_0 ($K_{NRT} = 10^{-7}$ dpa/s)	$5.6\cdot 10^{-4}$		
Fitting parameters (ϕ_m, ϕ^*)	1.9, 15.0		

diffusivity anisotropy will be measured by the correction factor $Z^* = (u + u^{-2}\sqrt{3 + u^6})/3$ with $u = (D_{ic}^{Zr}/D_{ia}^{Zr})^{1/6}$, where in further calculations we put $Z_{iI}^{j*} = Z_{iI}^j Z^*$, $Z_{vI}^{j*} = Z_{vI}^j Z^*$, and drop asterisk for convenience (to get more accurate description one can use vacancy diffusivity anisotropy in a manner similar to interstitial diffusion anisotropy).

In further calculations, we consider an Zr–1.5% Sn alloy as the main object to study. We vary irradiation temperature, sink strengths, and consider local loops distribution inside grains. The model parameters are taken from a fitting of experimental data of neutron irradiation of Zy-2 discussed in [36, 54]. Material parameters and fitting constants used in simulations are shown in Table 1. In further computation we put $\varepsilon_r = 0.95$ and use following values of defect clustering efficiencies: $\varepsilon_i^s = 0.5$, $\varepsilon_i^g = 0.17$, $\varepsilon_v^s = 0.55$, $\varepsilon_v^g = 0.05$ [34–36, 40, 63]. We take experimental value for network dislocation density equals to dislocation number density $(0.1–1.0)\cdot 10^{10}$ cm^{-2} in each crystallographic direction. The grain radius λ_{GB} we vary from 4 μm up to 10 μm. A distance from grain boundary is measured in dimensionless units $\delta = l/\lambda_{GB}$. Irradiation temperature varies in the interval 540–570 K. For the damage rate at irradiation by neutrons we take value $K_{NRT} = 10^{-7}$ dpa/s according to experimental data [54].

3. RESULTS

3.1. Dose Dependences Analysis

We start from dose dependences of loop number densities in both <*a*>- and <*c*>-directions obtained from the experimental data fitting shown in Fig. 1 (it is assumed that $N_{\mathrm{I}}^{m} = N_{\mathrm{V}}^{m}$). It follows those curves for both <*a*>- and <*c*>-type loop densities manifest saturation behaviour with a dose accumulation and relate well to experimental data [53, 54, 69]. Here one needs to note that data shown in [53, 69] correspond to the total loop number density, whereas in our case one gets the loop number density in one of equivalent directions as one-third of the total loop number density. Moreover, corrections caused by temperature increase result in a decrease in the number of <*a*>-type loops. By considering a case of negligibly small amount of <*c*>-type loops one finds that obtained dependences are comparable with those discussed in [34–36]: a transition to saturation regime for <*a*>-type loops occurs at doses around 4 dpa, whilst for <*c*>-type loops one has the transient behaviour at doses around 15 dpa with growth of $N_{\mathrm{V}}^{\mathrm{c}}$ from the critical dose of 3 dpa [5]; the difference only in values of both N_{I}^{a} and $N_{\mathrm{V}}^{\mathrm{c}}$ dictated by experimental observations [54].

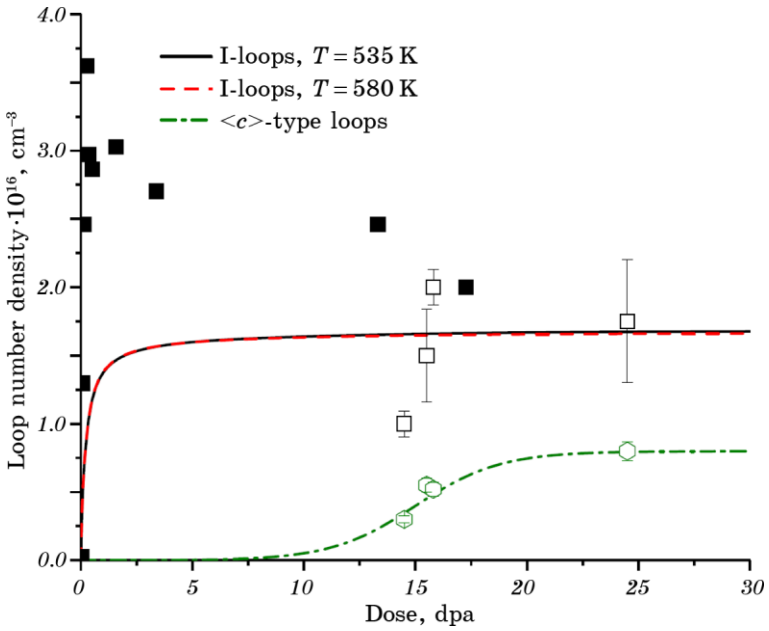

Fig. 1. Loop number densities in both <*a*>- and <*c*>-directions (solid, dashed and dash-dot curves) and experimental data ([53, 69] filled and empty squares for <*a*>-type loops and [54] empty diamonds for <*c*>-type loops).

Computed values of loop radii in each direction are shown in Fig. 2, *a*. It follows that interstitial loops emerge together with vacancy loops in <*a*>-direction (*cf.* solid and dash curves), whilst <*c*>-type loops grow above the critical dose 3 dpa from a cluster of the size not less than 5 nm.

At small doses (see insertion in Fig. 2, *a*) interstitial loops emerge first, vacancy loops appear after some incubation dose and grow faster than interstitial ones. At further dose accumulation one observes decreasing dynamics of <*a*>-type vacancy loop radius meaning metastability of these loops, interstitial loop size manifests increasing character only. A local decrease of <*c*>-type loops size is observed at doses related to transient regime of N_V^c (see Fig. 1). The same behaviour of <*c*>-type loop radius was observed in previous theoretical studies, where different model for loop number density was used [34–37]. It follows that <*a*>-type loop size does not exceed value of 5 nm at doses up to 1 dpa that relates well to the most of studies of Zr-based alloys at neutron irradiation at the same temperatures (see [5, 53]). A coexistence of vacancy and interstitial loops relates well to experimental observations (see [7, 8, 53, 69, 73]). By comparing <*a*>-type loop size at different doses one finds a difference in values up to 2–3 times, but the order of loop sizes is the same. The same is observed for <*c*>-type loop size. One needs to note that our model describes loop sizes in the same range as experiments. It relates mostly to different alloy compositions

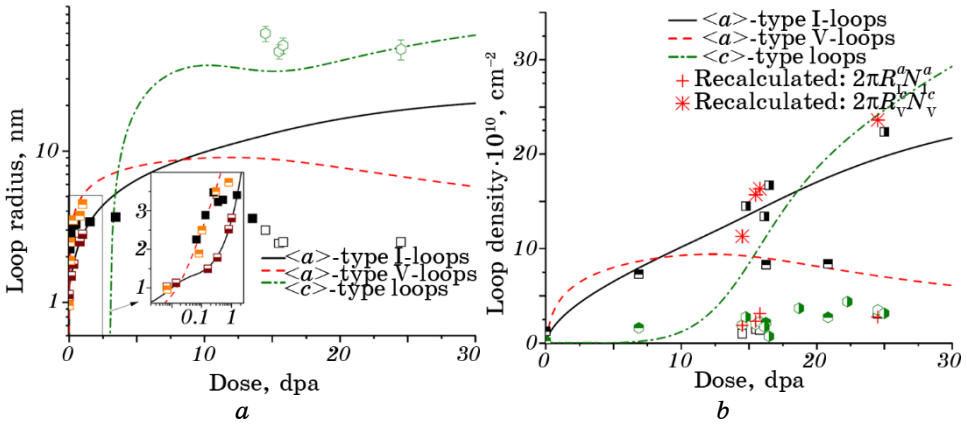

Fig. 2. Dose dependences of dislocation loop radii (*a*) and loop densities (*b*) (solid, dashed and dash-dot curves) and experimental data from [54, 69, 70–72] (empty and semi-empty markers). Recalculated data from experimental observations from [54] are shown with crosses and snowflakes. Square markers belong to <*a*>-type loops, diamond markers correspond to <*c*>-type loops. Results are obtained at $c_{Sn} = 1.5\%$, $T = 570$ K, $\lambda_{GB} = 7$ μm, $\rho_N^j = 0.7 \cdot 10^{10}$ cm^{-2}, $\delta = 0.5$.

and processing history, and possible synergetic effects of minor processes, which we neglect: emission of defects by loops, formation of defect complexes, their mobility, *etc*. The analogous situation is realized by considering values for loop densities shown in Fig. 2, *b*. Here, we obtain loop densities by using the standard definition $\rho_{\text{Г}}^{j} = 2\pi R_{\text{Г}}^{j} N_{\text{Г}}^{j}$.

In experiments (see empty markers from [54]), loop size, loop density and loop number density were measured that leads to differences in computed and measured values (see cross and snowflake markers in Fig. 2, *b*). This evidence is well seen by computing loop density by using experimental values for both loop size and loop number density. It results in a good correspondence with values obtained by our modelling. At the same time, obtained values for loop densities relate well to experimental data from [71].

Next, let us consider dose dependences of growth strains shown in Fig. 3. It follows that growth speeds in all Cartesian directions and values of $e^{x, y, z}$ is practically the same that predicts volume conservation. Generally obtained dependences relate well to data shown in [36]. In the top inset, one can observe that growth strains in X (Y) and Z directions differ at small doses. This effect is strongly related to an emergence of <*a*>-type vacancy loops, promoting deformation in Z direction. A strain induced by traps was computed as follows $e_{\text{T}} = (3\Omega - 2\Delta V_{\text{v}}) / 6\Omega$, where ΔV_{v} is relaxation volume [40]. The corresponding dose dependence is

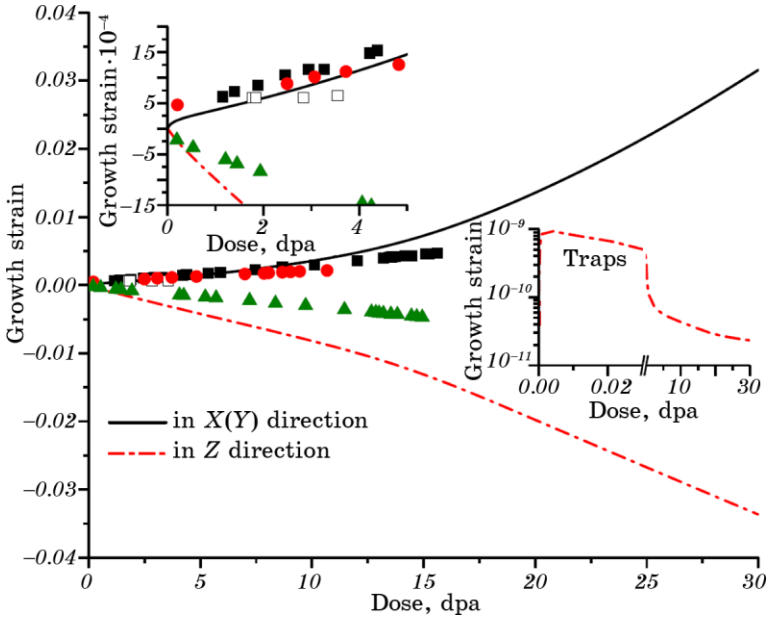

Fig. 3. Dose dependences of growth strains (experimental data are taken from [74]).

shown in the right inset in Fig. 3. It follows that effect of traps is negligibly small comparing to other mechanisms governing radiation growth phenomena. Values of growth strains are higher by absolute value than experimental data for single crystals [74]. This difference is caused by the presence of <*a*>-type vacancy loops giving a contribution to growth strains from one hand and grain boundaries effect resulting in additional contribution to growth strain rates, from the other one. Experimental studies of radiation growth in polycrystalline materials illustrate the same high values for growth strains (see, for example, [75, 76]). One should note that dose dependences of growth strains depend on texture [7, 75–77] that can explain a difference in the corresponding values. In our case, the texture is not considered, but a good agreement with experimental data is observed at doses up 6 dpa.

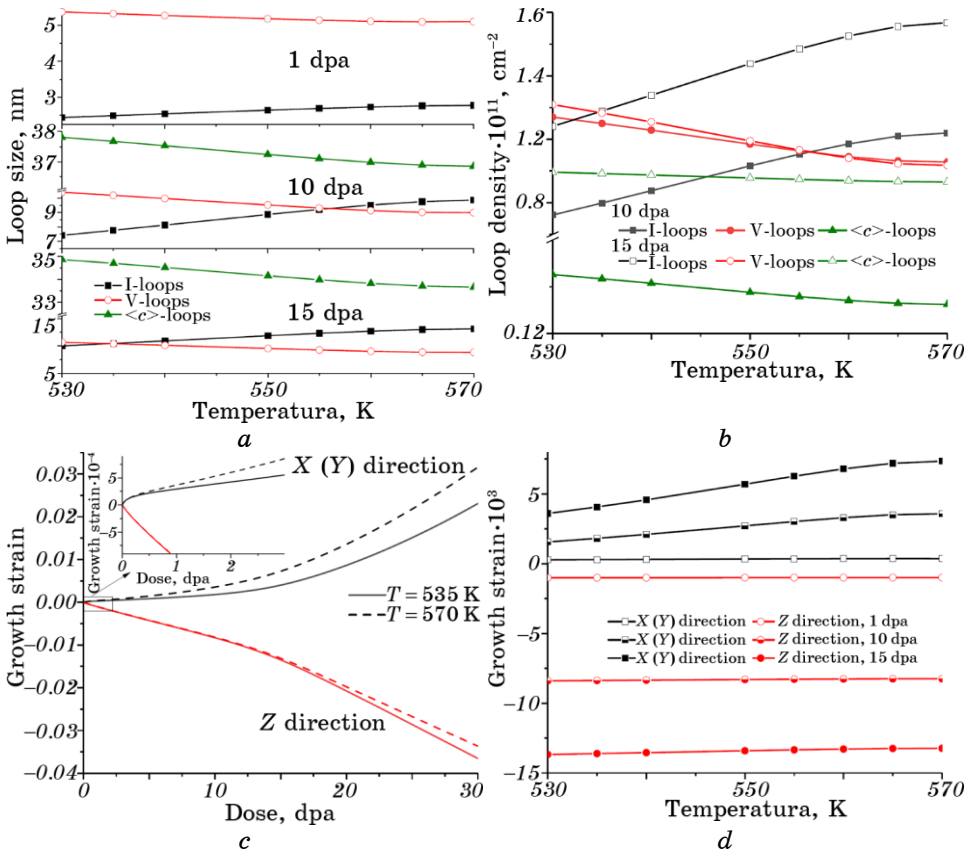

Fig. 4. Temperature dependences of loop radii (*a*), dislocation loop density (*b*), dose dependences of growth strains (*c*), and growth strains (*d*) at different doses. Results are shown at $c_{Sn} = 1.5\%$, $\lambda_{GB} = 7\ \mu m$, $\rho_N^j = 0.7 \cdot 10^{10}\ cm^{-2}$, $\delta = 0.5$.

From dose dependences shown above one concludes that a set of fitting parameters and main assumptions used in simulations are relevant to most of experimental data and theoretical models used previously to describe loops growth and radiation growth phenomena.

3.2. An Influence of Irradiation Temperature

By using protocols for dose dependences of all measured quantities, one can analyse the temperature influence onto dynamics of loop size, loop densities and growth strains. From results shown in Fig. 4, *a* it follows that an increase in the irradiation temperature results in growth of the interstitial loop size and decrease in the vacancy loop size. This effect becomes essential with dose accumulation, cf. panels at different doses in Fig. 4, *a*. An increase of the loop size with temperature was reported in experimental studies (see Refs. [5, 7, 51, 53, 69, 73, 78]). From Figure 4, *b*, one finds that the interstitial loop density increases with temperature, whilst vacancy loop densities of both <*a*>- and <*c*>-type loops decrease with temperature independently on dose. Dose dependences of growth strains at different temperatures illustrate a small difference in values of e^z at the temperature increase, whilst a difference in values of $e^{x, y}$ increases (see Fig. 4, *c*). This effect is caused by the corresponding dynamics of loop sizes. By considering temperature dependences of growth strains at different doses (see Fig. 4, *d*) it follows that at small doses there is no essential changes in lattice deformations. Observable changes are realized for growth strains in *X* and *Y* direction only at elevated doses.

3.3. An Effect of Grain Size

From obtained dose dependences shown in Fig. 5 one finds that an increase in grain size promotes growth of interstitial loop size associated with a decrease in <*a*>-type vacancy loop radius. It is related to a competition between interstitial and vacancy loops. By assuming that glissile interstitial clusters have a diffusivity comparable to diffusivity of self-interstitials one finds that the time scale for these clusters to attain grain boundaries as main sinks increases. It results in a growth of total network flux of defects to interstitial loops and an effective decrease of defect flux to <*a*>-type vacancy loops. At the same time, <*c*>-type loops grow faster in large grains.

From dependences of loop radii on grain size at different doses one finds that both kinds of <*a*>-type loops tend to the same value of 4 nm at small doses. With further dose accumulation the difference in loop radii increases up to 2.5–4 nm. The size of <*c*>-type loop increases with the grain size up to 10 nm at doses around 10 dpa. With further

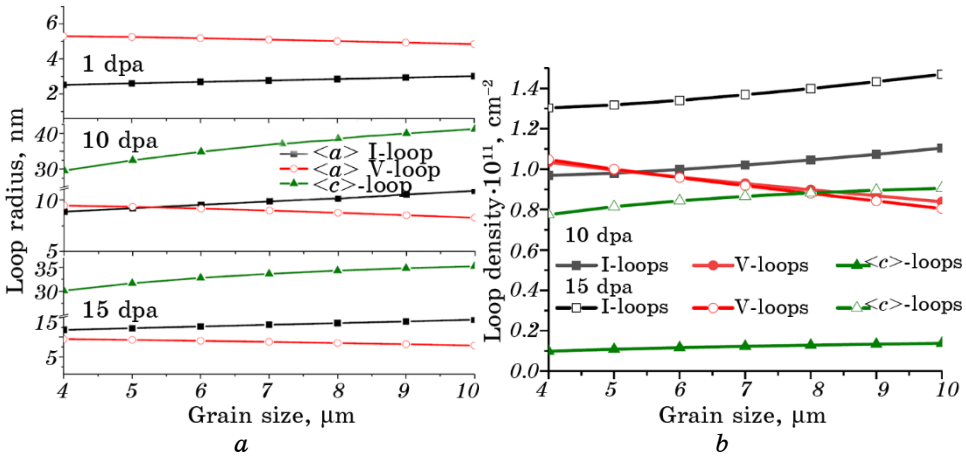

Fig. 5. Grain size dependences of loop radii (*a*) and loop density (*b*) at different doses. Results are shown for $c_{Sn} = 1.5\%$, $T = 570$ K, $\lambda_{GB} = 7$ μm, $\rho_N^j = 0.7 \cdot 10^{10}$ cm^{-2}, $\delta = 0.5$.

dose accumulation the loop size difference decreases down to 10 nm (see data for 15 dpa). At large doses there is no essential difference in loop radii. The corresponding loop densities shown at 10 dpa and 15 dpa indicate that interstitial loop densities manifest growing dependences with grain size growth, whereas vacancy <*a*>-loop density decreases and their density remains similarly the same, independently on accumulated dose (*cf.* lines with empty and filled circles). The density of <*c*>-type loops slightly increase with grain size at elevated doses only.

By considering dose dependences of growth strains (see Fig. 6, *a*) one finds that values of $e^{x, y, z}$ are lower in large grains at small doses. At elevated doses, one gets larger values of $e^{x, y}$ in large grains. The grain strain in *Z* direction remains small in large grains. The same results were observed experimentally [75]. One should note that such dynamics is affected by a prehistory of material and texture parameters. From Figure 6, *b* one finds that grain size dependences of growth strains in *X* (*Y*) directions are different at different doses: at small doses $e^{x, y}$ decay with the grain size. With the dose accumulation these growth strains manifest non-monotonic behaviour: a decrease in small grains and increase in large ones. It follows those values of growth strains in *Z*-direction increase monotonically with the grain size.

3.4. Loops Distribution inside the Grains

From physical viewpoint, grain boundaries are extremely powerful

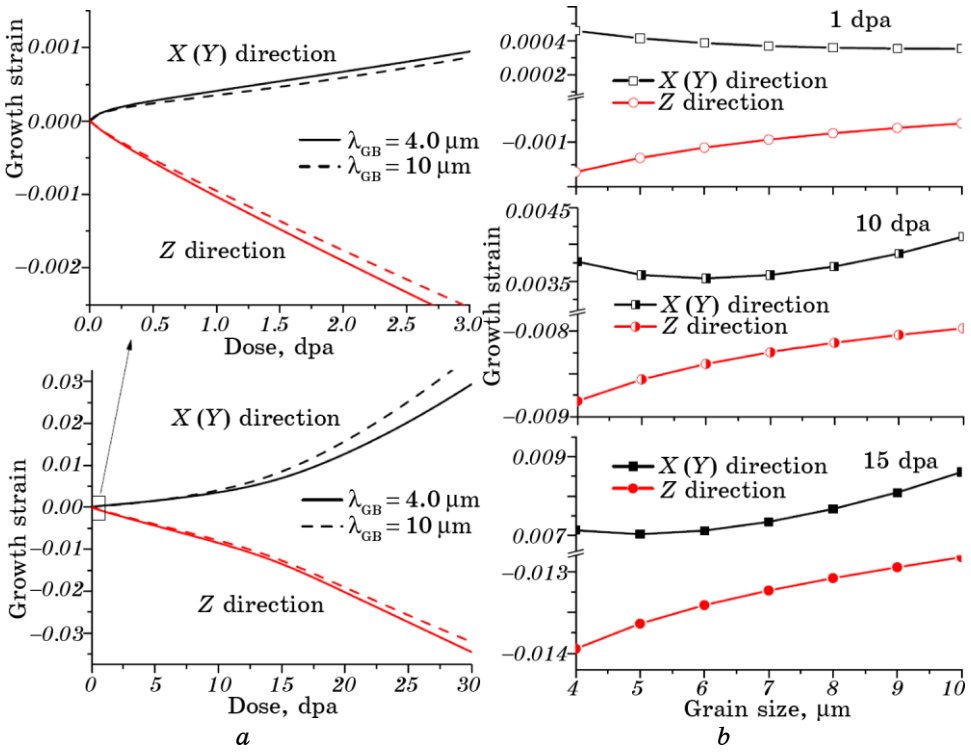

Fig. 6. Dose dependences of growth strains at different grain sizes (*a*) and grain size dependences of growth strains at different doses (*b*). Results are shown at $c_{Sn} = 1.5\%$, $T = 570$ K, $\rho_N^j = 0.7 \cdot 10^{10}$ cm^{-2}, $\delta = 0.5$.

sinks comparing to other ones due to they contain large amount of dislocation cores as separated sinks of point defects and their clusters. This effect is enforced by grains disorientation resulting in grain energy increase. Therefore, loops of different sizes will be located at different distances from grain boundaries. In our study, we consider the simplest case of grain characterized by one liner size λ_{GB} and study local distribution of loops inside grains by computing loop radii in different segments of grains located at dimensionless distance $\delta = l/\lambda_{GB} > 0$ from a grain boundary (the dimensionless distance δ cannot take zero value (in close proximity to the grain boundary); mathematically it is related to a divergence $\delta^{-1/2}$ of clusters sinks.). By using an initial loop size $R_{I,V}^{min}(0) \approx 0.65$ nm to scale the space, one can estimate the minimal value for the dimensionless distance as $\delta_{min} = R_{I,V}^{min}(0) / \lambda_{GB}^{min}$, where $\lambda_{GB}^{min} = 4$ μm.

Dose dependences of loop radii in different segments of grains are shown in Fig. 7, *a*. It follows that loops grow with different speeds and have different sizes depending on their location. In the grain centre

(solid lines at $\delta = 1$) interstitial loops are characterized by elevated values comparing to those located closer to grain boundaries (see dotted lines obtained at $\delta = 0.02$). The opposite picture is observed for <*a*>-type vacancy loops. In general, <*c*>-type loops manifest the same behaviour as interstitial loops: they are bigger in the grain centre segments and manifest complex growth dynamics. Loops of <*c*>-type are smaller in a vicinity of grain boundaries.

An essential difference in loop sizes (more than 1 nm) is observed only in a vicinity of the grain boundary at distances around 70% from the grain centre that is well seen from Fig. 7, *b*. Here, interstitial loops are of extremely small sizes due to fast diffusion of interstitials and their clusters toward grain boundaries (see curves with square markers). A lack of interstitials in these segments of grains makes possible a growth of <*a*>-type vacancy loops having larger size comparing to their size in the grain centre. Obtained results for local <*a*>-type loops distribution inside grains correspond well to data reported in experimental studies (see, for example, [79, 80]). In grain boundary seg-

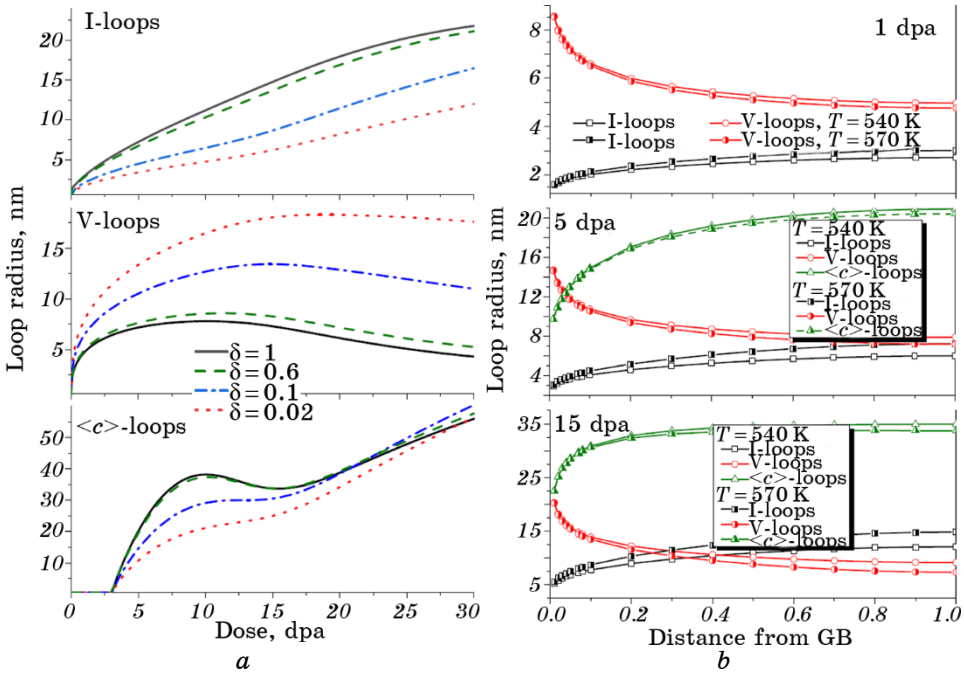

Fig. 7. Dose dependences of loop radii in different segments of grain located at distances δ from a grain boundary (*a*). Plots (*b*), (*c*) and (*d*) relate to local distribution of loop radius, loops densities and growth strains at different doses, respectively. Results are shown at $c_{Sn} = 1.5\%$, $T = 570$ K, $\lambda_{GB} = 7$ μm, $\rho_N^i = 0.7 \cdot 10^{10}$ cm^{-2}.

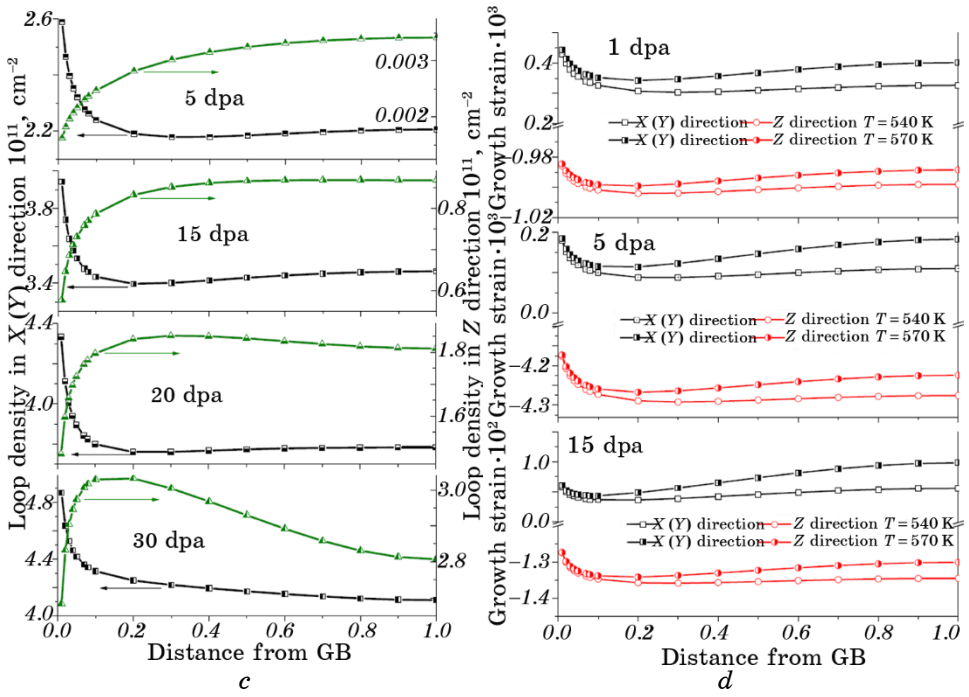

Continuation of Fig. 7.

ments the most of vacancies are captured by large <*a*>-type vacancy loops, therefore, <*c*>-type loops are characterized by smaller size comparing to already formed <*a*>-type loops. Out of grain boundaries they grow fast and the most of <*c*>-type loops attain equal size. The size of both kinds of <*a*>-type loops becomes equal with further dose accumulation; at elevated doses the size of interstitial loops exceeds vacancy loop size. In most of experimental studies it is reported that loop size distribution at doses around (10–15) dpa is mostly homogeneous (see, for example, [54]).

We have shown that this situation realized mostly in regions located outside grain boundaries. Such local description of loop growth results in a conclusion of local distribution of loop density as it is shown in Fig. 7, *c*. Here loop density in *X* (*Y*) direction manifests decreasing dependences with distance from the grain boundary. The difference in loop densities in the vicinity of grain boundary and grain segments is around 20% at 5 dpa. With the dose accumulation loop densities increase but a difference in their values remains around 20%. At elevated doses (see plot at 30 dpa) one finds only a decreasing character of corresponding dependences. Such a decrease in a vicinity of the grain boundary results to a decrease in <*a*>-type vacancy loop size. One gets

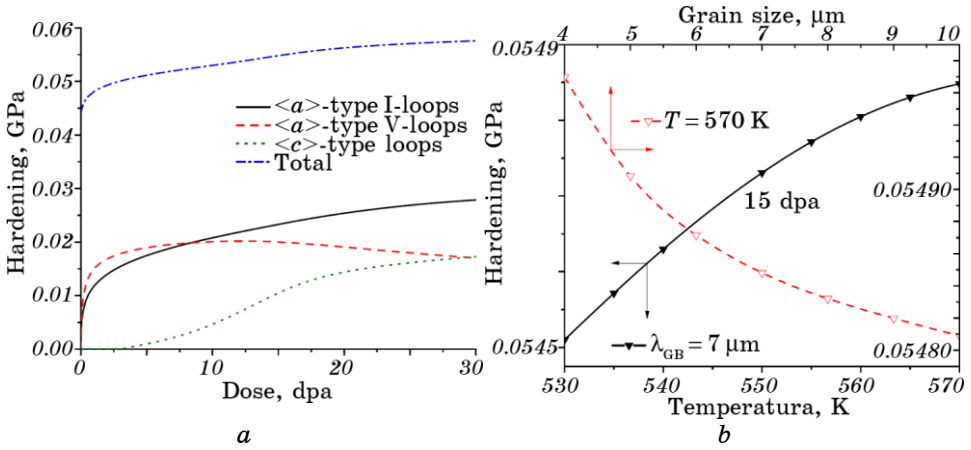

Fig. 8. Dose dependences of the hardening change caused by different kind of loops (results are obtained at $c_{Sn} = 1.5\%$, $T = 570$ K, $\lambda_{GB} = 7$ μm, $\rho_N^j = 0.7 \cdot 10^{10}$ cm^{-2}) (*a*). Dependences of total hardening change on temperature at $\lambda_{GB} = 7$ μm (filled triangles markers) and grain size at $T = 570$ K (empty triangle markers) at the accumulated dose 15 dpa (*b*).

an increasing character of the <*c*>-loop density at small doses. With the dose accumulation values of ρ^Z increase. A decreasing dynamic is observed in segments closer to grain boundaries (see plot at 30 dpa). The difference in loop densities inside the grain is around (10–15)%. Therefore, generally, one can operate with mean values with some errors suitable for experimental observation, but local loop sizes distribution results in local change of loop densities. Discussed locality in loops distribution over grain results in local deformation of grain at radiation growth. The corresponding dependences of growth strains on distance from grain boundary are shown in Fig. 7, *d*. Here elevated values of strains in *X* (*Y*) direction and low values of e^z in a vicinity of grain boundaries are caused by a presence of large vacancy loops of <*a*>-type. With a distance δ increase a competition of interstitial and vacancy loops promotes a decrease in $e^{x, y}$ and an increase in e^z by absolute value. Growth strains remain practically of the same value around grain centre segments.

3.5. Estimation of the Hardening

All defects formed and developed at irradiation serve as obstacles to free motion of dislocations resulting in an increase in hardening. Hence, in computations of the hardening as macroscopic characteristic one operates with averaged quantities (mean dislocation loop size) over the whole system. By using protocols of dose dependences of all com-

ponents of the hardening, one can get parametric dependences of hardening at fixed doses to elucidate an influence of main parameters controlling mechanical properties change of the studied alloys. The corresponding dose dependences of main components of the hardening and the total hardening are shown in Fig. 8, *a*. A growth of total hardening with dose accumulation is due to permanent growth of interstitial loops and <*c*>-type vacancy loops compensating a corresponding decrease induced by metastability of <*a*>-type vacancy loops.

Temperature and grain size dependences of total hardening shown in Fig. 8, *b* illustrate an increase in values of the yield strength with temperature and a slight decrease with grain size. Both these effects are strongly related to behaviour of mean loop sizes.

4. SUMMARY

We have generalized rate theory model to describe an evolution of defect structure and associated effects of radiation growth and hardening change during neutron irradiation in Zr–Sn alloys under reactor conditions. The model allows one to consider an influence of point defect clusters onto loop growth dynamics according to results of theoretical studies discussed in [6, 34–36]. We proposed a model for loop number densities evolution by taking into account mechanisms governing loops formation, nucleation and growth according to experimental data. A set of fitting parameters is related only to maximal values of number densities and their crossover dynamics. By considering dynamics of loop size a loops nucleation with network of dislocations is taken into account by considering an influence of domains localizing dislocations.

As shown, interstitial loops emerge at low doses, whereas vacancy <*a*>-type loops grow after small incubation dose. These loops attain the size of 5 nm at doses up to 1 dpa and coexist competing with each other at the studied temperature range. Interstitial loops manifest permanent grow (up to 20 nm at doses up to 30 dpa), whilst vacancy <*a*>-loops are metastable with maximal size around 10 nm. Loops of <*c*>-type emerge after critical dose of 3 dpa with minimal radius around 4–5 nm that is correlated with experimental data shown in [8]. They grow up to 50 nm at dose of 30 dpa. Obtained results relate well to experimental observations at small doses and correlate with novel experimental data at elevated doses [5, 53, 54, 69, 70–72].

It was shown that interstitial loops grow in size with temperature, whereas vacancy loops size decreases with temperature that relates well to experimental observations [5, 7, 51, 53, 69, 73, 78]. This effect determines temperature behaviour of growth strains: elongation in *X* (*Y*) directions and decrease of crystal shrinking in *Z* direction with temperature growth.

It was shown that large interstitial loops are realized in large grains (the same effect is observed for <*c*>-type loops), whereas vacancy <*a*>-type loops decrease in size in large grains due to competition in defect net flux to interstitial and vacancy loops of <*a*>-type. It was shown that growth strains behave in nonmonotonic manner with varying grain size and this behaviour depends on the accumulated dose. Obtained results are comparable with experimental data shown in [7, 75].

The proposed model is exploited to study local distribution of loop sizes inside grains. It was shown that a decrease in interstitial loop size and increase in <*a*>-type vacancy loop size in the vicinity of grain boundaries relate to a difference in mobility of corresponding point defects and their clusters and, therefore, in a competition between defect fluxes to these kinds of loops. As shown, homogeneous loop size distribution is observed out of grain boundaries. These results relate to discussions of experimental data [79, 80]. It was shown that local distribution of loops results in local deformation of the crystal.

By estimating mechanical properties change we have shown that the hardening grows with temperature and decrease with the grain size. Results of our modelling correlate well to the most of experimental data [7, 71, 75–77] and relate well to theoretical predictions [6, 28, 34–37].

We hope that obtained results correlated with experimental works will be useful to predict materials behaviour at different radiation conditions.

This work was supported by the National Natural Science Foundation of China (U2067218), Sichuan Science and Technology Program (2021JDGD0031), and the National Key Laboratory Foundation of Reactor Fuel and Materials (6142A06190510).

REFERENCES

1. C. Lemaignan, *Comprehensive Nuclear Materials* (Ed. R. J. M. Konings) (Elsevier: 2012), **vol. 2**, p. 217.
2. B. A. Cheadle, *Zirconium in the Nuclear Industry: 16th International Symposium* 2010, p. 67.
3. S. J. Zinkle, *Comprehensive Nuclear Materials* (Ed. R. J. M. Konings) (Elsevier: 2012), **vol. 1**, p. 65.
4. G. S. Was, *Fundamentals of Radiation Materials Science* (Berlin Heidelberg New York: Springer: 2007).
5. F. Onimus and J. L. Bechade, *Comprehensive Nuclear Materials* (Ed. R. J. M. Konings) (Elsevier: 2012), vol. **4**, p. 1.
6. S. I. Golubov, A. Barashev, and R. E. Stoller, *Comprehensive Nuclear Materials* (Ed. R. J. M. Konings) (Elsevier: 2012), vol. **1**, p. 357.
7. S. I. Choi and J. H. Kim, *Nucl. Eng. Tech.*, **45**, Iss. 3: 385 (2013).
8. Si-Mian Liu, Irene J. Beyerlein, and Wei-Zhong Han, *Nat. Commun.*, **11**: 5766

(2020).
9. M. Griffiths, M. H. Loretto, and R. E. Smallman, *J. Nucl. Mater.*, **115**, Iss. 2–3: 323 (1983).
10. Y. De Carlan, C. Regnard, M. Griffiths, D. Gilbon, and C. Lemaignan, *Zirconium in the Nuclear Industry: Eleventh International Symposium* (Eds. E. R. Bradley and G. P. Sabol) (West Conshohocken, PA: American Society for Testing and Materials: 1996), p. 638.
11. N. De Diego, Y. N. Osetsky, and D. J. Bacon, *J. Nucl. Mat.*, **374**, Iss. 1–2: 87 (2008).
12. V. Fidleris, R. P. Tucker, and R. B. Adamson, *Zirconium in the Nuclear Industry* (Eds. R. B. Adamson and L. F. P. Van Swam) (Philadelphia, PA: American Society for Testing and Materials: 1987), p. 49.
13. W. L. Bell, *J. Nucl. Mat.*, **55**, Iss. 1: 14 (1975).
14. Yu. N. Osetsky, D. J. Bacon, A. Serra, B. N. Singh, and S. I. Golubov, *J. Nucl. Mater.*, **276**, Iss. 1–3: 65 (2000).
15. G. D. Samolyuk, A. V. Barashev, S. I. Golubov, Yu. N. Osetsky, and R. E. Stoller, *Acta Mat.*, **78**: 173 (2014).
16. D. Kulikov and M. Hou, *J. Nucl. Mat.*, **342**, Iss. 1–3: 131 (2005).
17. V. O. Kharchenko and D. O. Kharchenko, *Cond. Mater. Phys.*, **16**: 13801 (2013).
18. L. Wu, V. O. Kharchenko, D. O. Kharchenko, and R. Pan, *Material Today Communications*, **26**: 101765 (2021).
19. N. De Diego, A. Serra, D. J. Bacon, and Yu. N. Osetsky, *Model. Simul. Mater. Sci. Eng.*, **19**: 035003 (2011).
20. V. P. Ramunni and A. M. F. Rivas, *Mater. Chem. Phys.*, **197**: 163 (2017).
21. D. J. Bacon, *J. Nucl. Mater.*, **159**: 176 (1988).
22. Yu. N. Osetsky, D. J. Bacon, and N. de Diego, *Metall. Mater. Trans. A*, **33**: 777 (2002).
23. D. J. Bacon, *J. Nucl. Mater.*, **206**, Iss. 2–3: 249 (1993).
24. C. H. Woo, *J. Nucl. Mater.*, **276**, Iss. 1–3: 90 (2000).
25. R. Pan, L. Wu, X. Wu, A. Tang, W. Zhang, W. He, B. Wen, Y. M. Ovcharenko, and D. O. Kharchenko, *Rad. Eff. Def. Solids*, **174**, Iss. 9–10: 752 (2019).
26. C. Domain, C. S. Becquart, and L. Malerba, *J. Nucl. Mater.*, **335**, Iss. 1: 121 (2004).
27. A. Hardouin Duparc, C. Moingeon, N. Smetniansky-de-Grande, and A. Barbu, *J. Nucl. Mater.*, **302**, Iss. 2–3: 143 (2002).
28. F. Christiaen and A. Barbu, *J. Nucl. Mater.*, **346**, Iss. 2–3: 272 (2005).
29. F. Christiaen and A. Barbu, *J. Nucl. Mater.*, **393**, Iss. 1: 153 (2009).
30. D. O. Kharchenko, V. O. Kharchenko, O. M. Shchokotova, X. Wu, B. Wen, L. Wu, and W. Zhang, *Rad. Eff. Def. Solids*, **173**, Iss. 7–8: 527 (2018).
31. D. O. Kharchenko, V. O. Kharchenko, A. I. Bashtova, V. V. Kupriienko, and L. Wu, *J. Appl. Phys.*, **129**, Iss. 3: 035104 (2021).
32. T. D. de la Rubia and M. W. Guinan, *J. Nucl. Mater.*, **174**, Iss. 2–3: 151 (1990).
33. C. H. Woo, B. N. Singh, and H. Heinisch, *J. Nucl. Mater.*, **174**, Iss. 2–3: 190 (1990).
34. S. I. Golubov, A. V. Barashev, R. E. Stoller, and B. N. Singh, *Zirconium in the Nuclear Industry: 17th International Symposium* (Eds. R. Comstock and P. Barberis) (West Conshohocken, PA: ASTM International: 2014), p. 729.
35. A. V. Barashev, S. I. Golubov, and R. E. Stoller, *J. Nucl. Mater.*, **461**: 85 (2015).
36. A. Patra, C. N. Tomé, and S. I. Golubov, *Philos. Mag.*, **97**, Iss. 23: 2018 (2017).

37. L. Wu, D. O. Kharchenko, V. O. Kharchenko, O. B. Lysenko, V. Kupriienko, S. Kokhan , I. A. Shuda, and R. Pan, *Cond. Mat. Phys.*, **23**, No. 1: 13604 (2020).
38. S. I. Golubov, A. V. Barashev, and R. E. Stoller, *Mat. Res. Soc.*, **1383**: 55 (2012).
39. B. Christiaen, C. Domain, L. Thuinet, A. Ambard, and A. Legris, *Acta Mater.*, **195**: 631 (2020).
40. R. H. Zee, A. Rogerson, G. J. C. Carpenter, and J. Watters, *J. Nucl. Mater.*, **120**: Iss. 2–3: 223 (1984).
41. B. N. Singh, S. I. Golubov, H. Trinkaus, A. Serra, Yu. N. Osetsky, and A. V. Barashev, *J. Nucl. Mater.*, **251**: 107 (1997).
42. M. J. Norgett, M. T. Robinson, and M. I. Torrens, *Nucl. Eng. Des.*, **33**, Iss. 1: 50 (1975).
43. B. N. Singh, V. Eldrup, S. J. Zinkle, and S. I. Golubov, *Philos. Mag. A*, **82**, Iss. 6: 1137 (2002).
44. E. J. Savino and C. E. Laciana, *J. Nucl. Mater.*, **90**, Iss. 1–3: 89 (1980).
45. A. Seeger and U. Gösele, *Phys. Lett. A*, **61**, Iss. 6: 423 (1977).
46. D. Walgraef, *Spatio-Temporal Pattern Formation* (New York–Berlin–Heidelberg: Springer-Verlag: 1996).
47. J. Rest and G. L. Hofman, *J. Nucl. Mater.*, **277**, Iss. 2–3: 231 (2000).
48. N. Hanses and D. Kuhlmann-Wilsdorf, *Mater. Sci. Eng.*, **81**: 141 (1986).
49. S. R. MacEwen and G. J. C. Carpenter, *J. Nucl. Mater.*, **90**, Iss. 1–3: 108 (1980).
50. G. J. C. Carpenter, R. H. Zee, and A. Rogerson, *J. Nucl. Mater.*, **159**: 86 (1988).
51. A. Jostsons, P. M. Kelly, R. G. Blake, and K. Farrell, *Effects of Radiation on Structural Materials* (Eds. J. A. Sprague and D. Kramer) (West Conshohocken, PA: American Society for Testing and Materials: 1979), p. 46.
52. V. N. Shishov, A. V. Nikulina, V. A. Markelov, M. M. Peregud, A. V. Kozlov, S. A. Averin, S. A. Kolbenkov, A. E. Novoselov, *Zirconium in the Nuclear Industry: Eleventh International Symposium* (West Conshohocken, PA: American Society for Testing and Materials: 1996), p. 603.
53. D. O. Northwood, R. W. Gilbert, L. E. Bahlen, P. M. Kelly, R. G. Blake, A. Jostsons, P. K. Madden, D. Faulkner, W. Bell, and R. B. Adamson, *J. Nucl. Mater.*, **79**, Iss. 2: 379 (1979).
54. A. Harte, D. Jädernäs, M. Topping, P. Frankel, C. P. Race, J. Romero, L. Hallstadius, E. C. Darby, and M. Preuss, *Acta Mater.*, **130**: 69 (2017).
55. D. Fainstein-Pedreaza, E. J. Savino, and A. J. Pedraza, *J. Nucl. Mater.*, **73**, Iss. 2: 151 (1978).
56. H. L. Yang, Y. Matsukawa, S. Kano, Z. G. Duan, K. Murakami, and H. Abe, *J. Nucl. Mater.*, **481**: 117 (2016).
57. R. C. Rau and J. Moteff, *Rad. Eff.*, **8**, Iss. 1–2: 99 (1971).
58. J. H. Keller, *Trans. ASM*, **47**: 157 (1955).
59. G. R. Odette and D. Frey, *J. Nucl. Mater.*, **85–86**, Part 2: 817 (1979).
60. C. H. Woo, *J. Nucl. Mater.*, **159**: 237 (1988).
61. C. H. Woo, *Handbook of Materials Modeling*, (Ed. S. Yip) (Springer: 2005), p. 959.
62. R. C. Pasianot and A. M. Monti, *J. Nucl. Mater.*, **264**, Iss. 1–2: 198 (1999).
63. C. H. Woo and X. Liu, *Phil. Mag.*, **87**, Iss. 16: 2355 (2007).
64. H. Wen and C. H. Wen, *J. Nucl. Mater.*, **420**, Iss. 1–3: 362 (2012).
65. W. Franck, *J. Nucl. Mater.*, **159**: 122 (1988).
66. A. D. King, G. M. Hood, and R. A. Holt, *J. Nucl. Mater.*, **185**, Iss. 2: 174 (1991).

67. R. Pan, A. Tang, Y. Wang, X. Wu, and L. Wu, *Comput. Cond. Mater.*, **10**: 22 (2017).
68. P. Ehrhart and B. Schönfeld, *Metals* (Eds. J. I. Takamura, M. Doyama, and M. Kiritani) (Amsterdam: 1982), p. 47.
69. D. O. Northwood, *Atomic Energy Rev.*, **15**: 547 (1977).
70. R. A. Holt, A. R. Causey, N. Christodoulou, M. Griffiths, E. T. C. Ho, C. H. Woo, *Nuclear Industry: Eleventh International Symposium* (Eds. E. R. Bradley and G. P. Sabol) (American Society for Testing and Materials: 1996), p. 623.
71. T. Seymour, P. Frankel, L. Balogh, T. Ungár, S. P. Thompson, D. Jädernäs, J. Romero, L. Hallstadius, M. R. Daymond, G. Ribárik, and M. Preuss, *Acta Mater.*, **126**: 102 (2017).
72. Zh. Yao, M. Daymond, S. Di, and Y. Idrees, *Appl. Sci.*, **7**, Iss. 8: 854 (2017).
73. D. O. Northwood and R. W. Gilbert, *Rad. Eff.*, **22**, Iss. 2: 139 (1974).
74. G. J. C. Carpenter, R. H. Zee, and A. Rogerson, *J. Nucl. Mater.*, **159**: 86 (1988).
75. A. Rogerson, *J. Nucl. Mater.*, **159**: 43 (1988).
76. R. B. Adamson, *American Society for Testing and Materials*, **633**: 326 (1977).
77. M. Griffiths, R. W. Gilbert, and V. Fidleris, *Zirconium in Nuclear Industry: Eighth International Symposium* (Eds. L. F. P. Van Swan and C. M. Eucken) (Philadelphia: American Society for Testing and Materials: 1989), p. 658.
78. C. Hellio, C. H. de Novion, and L. Boulanger, *J. Nucl. Mater.*, **159**: 368 (1988).
79. M. Griffiths, R. W. Gilbert, and C. E. Coleman, *J. Nucl. Mater.*, **159**: 405 (1988).
80. H. Yu, Zh. Yao, Y. Idrees, H. K. Zhang, M. A. Kirk, and M. R. Daymond, *J. Nucl. Mater.*, **491**: 232 (2017).